Accurate description of high-order phonon anharmonicity and lattice thermal conductivity from molecular dynamics simulations with machine learning potential

Yulou Ouyang, Cuiqian Yu, Jia He [ORCID], Pengfei Jiang, Weijun Ren, and Jie Chen [ORCID][*]

Center for Phononics and Thermal Energy Science, China–EU Joint Lab for Nanophononics, MOE Key Laboratory of Advanced Micro-structured Materials, School of Physics Science and Engineering, Tongji University, Shanghai 200092, People's Republic of China

Phonon anharmonicity is critical for accurately predicting the material's thermal conductivity (κ). However, its calculation based on the perturbation theory is a difficult and time-consuming task, especially for the high-order phonon scattering process. In this work, using cubic boron arsenide (BAs) and diamond as examples, we combine the machine learning potential (MLP) with molecular dynamics simulations to predict κ and assess the effect of anharmonicity on thermal transport properties. A MLP based on the matrix tensor algorithm is developed in this work, which can accurately describe lattice dynamics behaviors in both BAs and diamond. The phonon spectral energy density analysis reveals that MLP can effectively capture both the phonon mode softening and the linewidth broadening induced by the anharmonicity at finite temperatures in both materials. Compared to diamond, BAs exhibits a stronger anharmonicity revealed by the larger deviation from equilibrium position and more pronounced phonon broadening effect, especially at high temperatures. Furthermore, based on the phonon Boltzmann transport equation and three-phonon scattering process, our calculation results demonstrate that the accuracy of the MLP in predicting the κ is comparable to that of density-functional theory calculations for both diamond and BAs. However, this framework can only predict κ of diamond in agreement with experimental measurements, but significantly overestimates the κ of BAs compared to the experimental results, due to the significant impact of high-order phonon scattering process in BAs. In contrast, the κ values predicted by equilibrium molecular dynamics simulations combined with MLP agree well with experimental values for both BAs and diamond. Our study suggests that molecular dynamics simulation combined with MLP is a reliable and computationally efficient tool to account for full orders of anharmonicity and provide accurate predictions of material's thermal conductivity without any *a priori* knowledge of the importance of high-order phonon anharmonicity.

I. INTRODUCTION

Understanding thermal transport in materials [1,2] is important for both heat management [3,4] and thermoelectrics [5,6]. Various phonon scattering mechanisms, such as lattice anharmonicity [7–9], substrate [10], isotope [11], and defect [12], should be considered in order to accurately predict the lattice thermal conductivity (κ) in realistic materials. Among these factors, the lattice anharmonicity is the dominant factor that determines the intrinsic κ in semiconducting crystals. As the leading-order anharmonicity, the three-phonon (3ph) scattering process has been treated for a long time as the primary origin for the anharmonic phonon-phonon interactions, until recent theoretical works [7,13,14] revealed the importance of high-order phonon scattering process in certain semiconductors with wide phononic band gaps.

For instance, when only considering the 3ph process and isotope scattering, Lindsay *et al.* [15] predicted based on the Peierls-Boltzmann transport equation (PBTE) that κ of boron arsenide (BAs) reaches $\sim$2200 Wm^{-1}K^{-1} at room temperature. Surprisingly, Feng *et al.* [7] demonstrated through PBTE calculations that including high-order phonon scatter-

ing processes such as four-phonon (4ph) scattering, which was previously considered to be negligible, can drastically reduce the room temperature κ to 1400 Wm^{-1}K^{-1} in BAs, due to the substantially enhanced phonon-phonon scattering via the 4ph process. Their prediction of κ in BAs was later confirmed by experimental studies [16–18].

However, due to the enormous computational cost, calculating high-order interatomic force constants (IFCs) based on density-functional theory (DFT) remains a challenging task. In this regard, machine learning potential (MLP) is a promising alternative to accelerate the calculation of IFCs and save computational costs, which has been demonstrated to have comparable accuracy as DFT calculations when computing the lattice thermal conductivity based on PBTE framework [19,20]. On the other hand, prior to such expensive PBTE calculations, there still lacks a criterion to determine *a priori* whether the high-order phonon scattering process is important in the perturbative treatment of PBTE framework. More importantly, a recent theoretical study [8] reveals that the temperature effects on the IFCs should be seriously considered, which further enhances the complexity and computational cost for treating high-order phonon anharmonicity in PBTE framework.

On the other hand, molecular dynamics (MD) simulations can implicitly incorporate anharmonic interactions to all

*[*]jie@tongji.edu.cn

orders, and simulate various realistic factors existing in experiments, such as defect, roughness, strain, grain boundary, and so on. As a result, it has been widely used to study the thermal transport in various systems [21–24], and can provide reliable prediction of lattice thermal conductivity [25]. More importantly, the quantum correction [26] to MD simulation is negligible at high temperatures where high-order anharmonicity is important, making MD simulation an ideal tool to tackle this problem. Although the accuracy of MD prediction depends critically on the empirical potentials used in the simulations [27], recent studies demonstrate that MLP can describe the atomic interactions with a high accuracy comparable to that of DFT calculations [28–30].Very recently, Liu *et al.* [31] utilized MD simulations combined with MLP to study the temperature-dependent thermal conductivity of SnSe and the underlying physical mechanism, in which the roles of four-phonon scatterings are also identified. Furthermore, our previous work [32] has demonstrated that the MLP has the significant advantage over the empirical potential in the sense that the trained MLP can achieve accurate predictions of multiple-target physical properties simultaneously, which is one of the major limitations that most empirical potentials face. These advantages make MD simulation an ideal tool to tackle the problem of high-order anharmonicity.

In this work, we examine the validity of MLP-based MD simulations for studying the impact of high-order anharmonicity on thermal transport in semiconducting crystals. Two kinds of bulk materials, diamond and BAs, are considered in this study, which correspond to two representative scenarios where the effect of high-order lattice anharmonicity is relatively weak and strong, respectively. The κ values of diamond and BAs are computed based on equilibrium molecular dynamics (EMD) simulations with moment tensor potential (MTP), and are further benchmarked with experimental results and PBTE predictions limited to three-phonon process. The effect of high-order anharmonicity is further studied via the atomic displacement and phonon spectral energy density (SED) analysis.

The rest of the paper is organized as following: Sec. II describes the theoretical methods used in this work, which includes the training of MTP based on the results of *ab initio* molecular dynamics (AIMD), the calculation of κ based on PBTE and/or MD simulations, and the calculation detail of SED analysis. Then, the main results are discussed in Sec. III. To show the accuracy of our MTP, in Secs. III A and III B, we compute the energy, atomic force, and phonon dispersion for both BAs and diamond by using the developed MTP and DFT calculations, respectively. In Secs. III C and III D, MD simulations based on MTP are performed to explore the high-order phonon anharmonicity and compute κ of BAs and diamond. Finally, we provide a summary and conclude this work in Sec. IV.

II. METHODS

A. Construction of a moment tensor potential

1. AIMD simulations for data generation

The Vienna *Ab initio* Simulation Package (VASP) code [33,34] with potpaw_PBE.54 pseudopotentials was used to perform AIMD simulations for collecting the energies and atomic forces as training datasets. The system size of BAs and diamond for AIMD calculations was $3 \times 3 \times 3$ conventional cells, containing 216 atoms. The cutoff energies of 520 and 600 eV were used for BAs and diamond, respectively. A $2 \times 2 \times 2$ Γ-centered grid of k points in the irreducible Brillouin zone was used. To fully consider the effect of temperature on structures, AIMD was performed with the isothermal-isobaric (*NPT*) ensemble from 0 to 1000 K. The time step was 0.5 fs and the total step was 2000 steps, generating 2000 atomic configurations and corresponding data (forces, energies, and stresses) that were used to train MTP.

2. Training of machine learning potential

The MTP developed by Shapeev [35] is used in this work to describe the interatomic interaction in BAs and diamond, since MTP has the advantages of balanced accuracy and computational efficiency compared with other machine learning potentials [36]. In MTP model, the total energy of a configuration m (E_m^{MTP}) is written as [35]

$$E_m^{\mathrm{MTP}} = \sum_{i=1}^{N} V_m(\mathbf{n}_i), \tag{1}$$

where $V_m(\mathbf{n}_i)$ is the function of ith atomic environment $\mathbf{n}_i$, and N represents the total number of atoms in the configuration m. The function V is given by a linear combination of a set of basic functions B_α [35],

$$V(\mathbf{n}_i) = \sum_{\alpha} \xi_\alpha B_\alpha(\mathbf{n}_i). \tag{2}$$

The basic functions B_α are constructed with all the possible contractions of the moment tensors descriptors $M_{\mu,\nu}(\mathbf{n}_i)$ defined as [35]

$$M_{\mu,\nu}(\mathbf{n}_i) = \sum_{j=1}^{N_k} f_\mu(|r_{ij}|, z_i, z_j) \underbrace{\mathbf{r}_{ij} \otimes \ldots \otimes \mathbf{r}_{ij}}_{\nu \text{ times}}, \tag{3}$$

where $f_\mu(|r_{ij}|, z_i, z_j)$ and $\underbrace{\mathbf{r}_{ij} \otimes \ldots \otimes \mathbf{r}_{ij}}_{\nu \text{ times}}$ are the radial and angular part of MTP, respectively. $|r_{ij}|$ represents the distance between atom i and j, and N_k is the number of atoms in the neighborhood environments of the ith atom. z_i and z_j represent the atomic types of atom i and j, respectively. The symbol $\otimes$ denotes the outer product of vectors. More details about the construction of B_α can be found in Ref. [37].

The parameter ξ_α in Eq. (2) is a set of coefficients that can be obtained by minimizing the difference between E_m^{MTP} and the AIMD energy (E_m^{AIMD}). The same method is also used to compute the atomic force $f_{m,i}^{\mathrm{MTP}}$ and stress σ_m^{MTP}. Finally, the parameters of MTP can be obtained by solving the minimization problem [35],

$$\sum_{m=1}^{M} \left[w_e \left(E_m^{\mathrm{AIMD}} - E_m^{\mathrm{MTP}} \right)^2 + w_f \sum_{i}^{N} \left| f_{m,i}^{\mathrm{AIMD}} - f_{m,i}^{\mathrm{MTP}} \right|^2 \right.$$
$$\left. + w_s \left| \sigma_m^{\mathrm{AIMD}} - \sigma_m^{\mathrm{MTP}} \right|^2 \right] \rightarrow \min, \tag{4}$$

where M is the number of the configurations in the training dataset, and w_e, w_f, and w_s are the weight factors for the energy, force, and stress, respectively.

B. Calculation of thermal conductivity

1. PBTE method

We used VASP code combined with PHONOPY code [38] and *thirdorder.py* script [39] to calculate the second-order (2-rd) and third-order (3-rd) IFCs for BAs and diamond. A set of supercells containing $2 \times 2 \times 2$ conventional cells was used to compute IFCs, and the Monkhorst-Pack k mesh of $5 \times 5 \times 5$ and $2 \times 2 \times 2$ is used to sample the irreducible Brillouin zone for the calculations of 2-rd and 3-rd IFCs, respectively. The cutoff energies of 520 eV and 600 eV were used for BAs and diamond, respectively.

In the PBTE framework, the thermal conductivity $\kappa^{\alpha\beta}$ is calculated by ShengBTE code [39] as

$$\kappa^{\alpha\beta} = \frac{1}{k_B T^2 \Omega N} \sum_\lambda n_0(n_0 + 1)(\hbar \omega_\lambda)^2 v_\lambda^\alpha F_\lambda^\beta, \quad (5)$$

where N, T, k_B, and Ω are the number of wave-vector points in the first Brillouin zone, temperature, the Boltzmann constant, and the volume of the unit cell, respectively. n_0 is the equilibrium Bose-Einstein distribution function, λ represents the phonon mode at wave vector $\mathbf{k}$ and branch index s. $\hbar$ represents the reduced Planck constant, and v_λ^α is the group velocity of λ along the αth direction. A q mesh of $30 \times 30 \times 30$ was used in ShengBTE for sampling the first Brillouin zone. In the PBTE calculation, only the 3ph scattering process is considered. The final κ is averaged over the three diagonal terms of the $\kappa^{\alpha\beta}$ tensor. More details about PBTE calculation can be found in our previous works [40,41].

2. EMD simulations

The developed MTP is used to perform EMD simulations based on the LAMMPS package [42]. In EMD simulation, κ can be obtained from the Green-Kubo formula as [43–45]

$$\kappa = \frac{1}{3k_B \Omega T^2} \sum_{\alpha=1}^{3} \int_0^\infty \langle J_\alpha(0) J_\alpha(t) \rangle dt, \quad (6)$$

where J_α represents the heat current along the αth direction. The heat current vector $\mathbf{J}$ is defined as

$$\mathbf{J} = \sum_i \mathbf{v}_i E_i + \sum_i \sum_{j \neq i} \mathbf{r}_{ij} \left(\frac{\partial U_j}{\partial \mathbf{r}_{ij}} \cdot \mathbf{v}_i \right) \quad (7)$$

where E_i, U_j, and $\mathbf{r}_{ij}$ are the total energy of ith atom, potential energy of jth atom, and position vector between atom i and j, respectively. The time step is set as 0.5 fs, and periodic boundary conditions are used in all directions. A supercell of $8 \times 8 \times 8$ unit cells (8 atoms per unit cell) is used for both BAs and diamond, which is sufficiently large according to the previous study [46]. In each simulation, the system is first equilibrated for 200 ps in the canonical (*NVT*) ensemble. The heat current is then recorded for 6 ns in the microcanonical (*NVE*) ensemble. The final κ is the average value over 30 independent EMD simulations with different initial conditions.

C. Spectral energy density

The SED method is a useful approach to estimate the phonon lifetimes from MD simulations including full order anharmonicity. The phonon SED $\Phi(\mathbf{k}, \omega)$ at wave vector $\mathbf{k}$ and frequency ω can be calculated as [47]

$$\Phi(\mathbf{k}, \omega) = 2 \sum_s^{3n} \lim_{\tau_0 \to \infty} \frac{1}{2\tau_0}$$
$$\times \left| \frac{1}{\sqrt{2\pi}} \int_0^{\tau_0} \dot{q}\binom{\mathbf{k}}{s}; t \exp(-i\omega t) dt \right|^2, \quad (8)$$

where $\dot{q}(^{\mathbf{k}}_s; t)$ is the time derivative of the normal-mode coordinate given by [47]

$$\dot{q}\binom{\mathbf{k}}{s}; t = \sum_{\alpha, b, l}^{3, n, N} \sqrt{\frac{m_b}{N}} \dot{u}_\alpha \binom{l}{b}; t \, e^* \binom{\mathbf{k} \ b}{s \ \alpha} \times \exp\left[i\mathbf{k} \cdot \mathbf{r}_0 \binom{l}{0} \right]. \quad (9)$$

Here, $e^*(^{\mathbf{k} \ b}_{s \ \alpha})$ is the conjugation of phonon mode eigenvector for the αth component, N represents the total number of unit cells in MD simulations, n is the total number of atoms in the unit cell, and m_b is the mass of the bth atom. $\mathbf{r}_0(^l_0)$ is the equilibrium position vector for the lth unit cell, and $\dot{u}_\alpha(^l_b; t)$ is the velocity of the bth atom in the α direction, which can be obtained directly from MD simulation.

In MD simulation, the total integration time τ_0 is set as 500 ps, and the time step is 0.5 fs. The SED calculations are performed on a supercell with periodic boundary conditions in the *NVE* ensemble. To make the discrete wave vectors commensurate with the supercell size, SED curves along the $\Gamma - X$ (x) direction, $X - K$ (y) direction, $K - \Gamma$ (x-y plane diagonal) direction, and $\Gamma - M$ (cubic diagonal) direction are calculated, using supercells containing $40 \times 2 \times 2$, $2 \times 40 \times 2$, $20 \times 20 \times 2$, and $8 \times 8 \times 8$ unit cells, respectively.

III. RESULTS AND DISCUSSION

A. Energy and atomic force

In this work, the complete dataset obtained from AIMD simulations (see Sec. II) is randomly divided into two parts: a training set (80%) and a validation set (20%). The training set is used to train the MTP, and the training process is performed by using the MLIP package [37]. The validation set is used to evaluate the accuracy of MTP in predicting the energy and atomic force.

After training the MTP, we calculate the root-mean-square error (RMSE) of energy and atomic force by comparing the data in the validation set and the predictions from MTP. Figure 1 shows the comparison of the energy and atomic force between MTP and DFT calculations. For BAs and diamond, the RMSE of energy per atom is 0.237 ± 0.084 meV/atom and 0.135 ± 0.062 meV/atom, respectively, while the RMSE of atomic force is 0.0197 ± 0.0074 eV/Å and 0.0217 ± 0.0048 eV/Å, respectively. Moreover, we have further verified that our sampling configurations are sufficiently large to ensure a convergent accuracy (see Fig. S1 in Supplemental Material [48]). The small RMSE values for both energy and
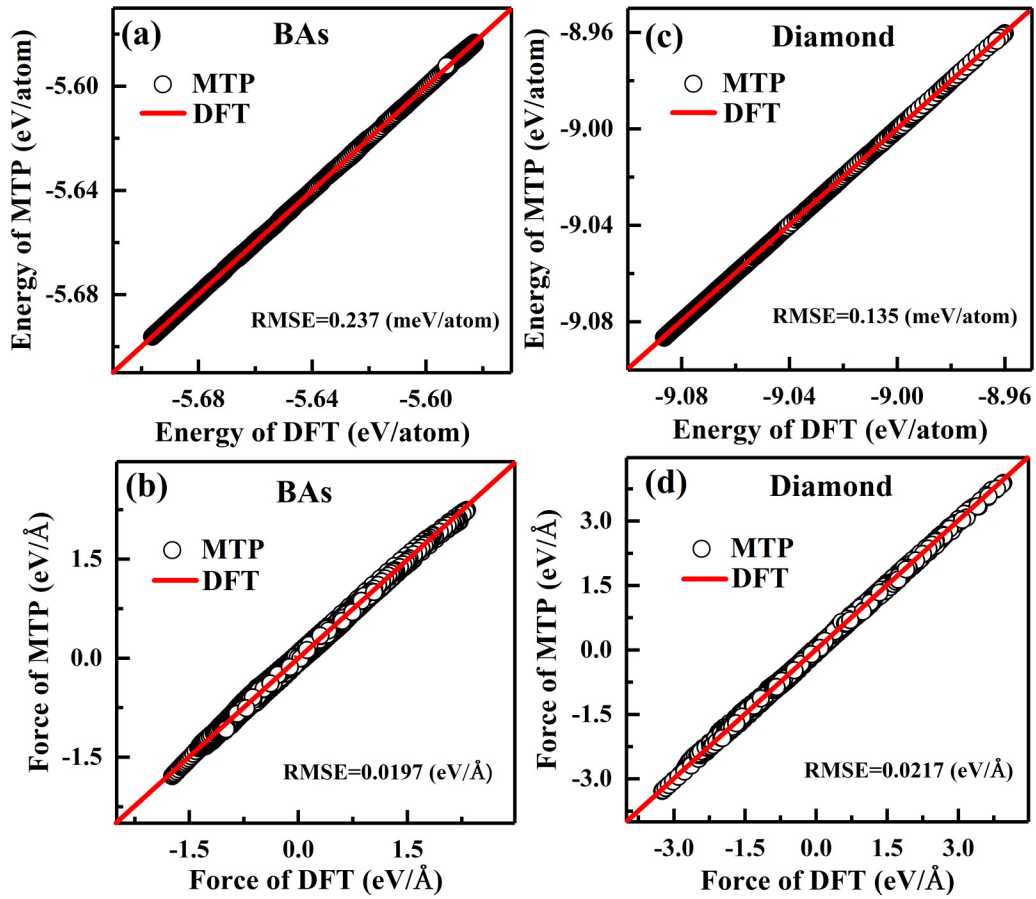
FIG. 1. Comparisons of energy per atom and atomic force between MTP and DFT calculations for BAs (a), (b) and diamond (c), (d). The RMSE is obtained by comparing the data between MTP and DFT calculations.

atomic force demonstrate that our MTP model has a high accuracy in reproducing the potential-energy surface comparable to DFT calculations, which has been demonstrated to ensure the accurate predictions of multiple-target physical properties [32].

B. Phonon dispersion

As a harmonic property, phonon dispersion is an important concept to understand the intrinsic phonon transport mechanism in the material. It contains diverse phonon information, including phonon band structure, group velocity, and phonon scattering phase space. To this end, we compute the phonon dispersion for both BAs and diamond by using the PHONOPY code [38], based on the 2-rd IFCs calculated from MTP, DFT, and the empirical Tersoff potential [49], respectively. The optimized Tersoff potential parameters for BAs and diamond are obtained from Refs. [50,51], respectively.

As shown in Fig. 2, the phonon dispersion predicted by Tersoff potential (dotted line) deviates substantially from DFT calculations (dashed line), especially for optical phonon branches. In particular, the optical phonon frequencies in BAs ($\sim$20 THz) are overpredicted by around 50% with Tersoff potential ($\sim$30 THz). Although the optical phonons contribute little to total thermal conductivity due to the relatively small group velocity, they can indirectly determine the thermal transport by affecting the three-phonon

scattering processes that involve optical phonons, such as acoustic+acoustic$\rightarrow$optical, and acoustic+optical$\rightarrow$optical. Therefore, the accuracy of the optical phonon branches can indirectly affect the accuracy of thermal conductivity predictions [32], which is also important as the acoustic phonon branches and thus should be accurately described.

In contrast, the phonon dispersion predicted by MTP (solid line) shows excellent agreement with that predicted by the DFT calculations (dashed line) for both BAs and diamond. More importantly, such excellent agreement is valid for all phonon branches, including the optical phonon branches. The agreement between MTP and DFT results validates the accuracy of MTP in reproducing the phonon dispersion for all phonon branches, which is a vital prerequisite to describe the energy and momentum conservation in phonon-phonon scattering processes for the prediction of κ.

C. Anharmonic phonon properties

1. Atomic vibration

A thorough understanding of microscopic properties from the atomic-scale perspective is of great significance to understand the physical origin of the macroscopic properties. In semiconductors or insulators, heat is mainly transported in the form of lattice vibrations (phonon). Therefore, based on MD simulations combined with MTP, we further investigate the
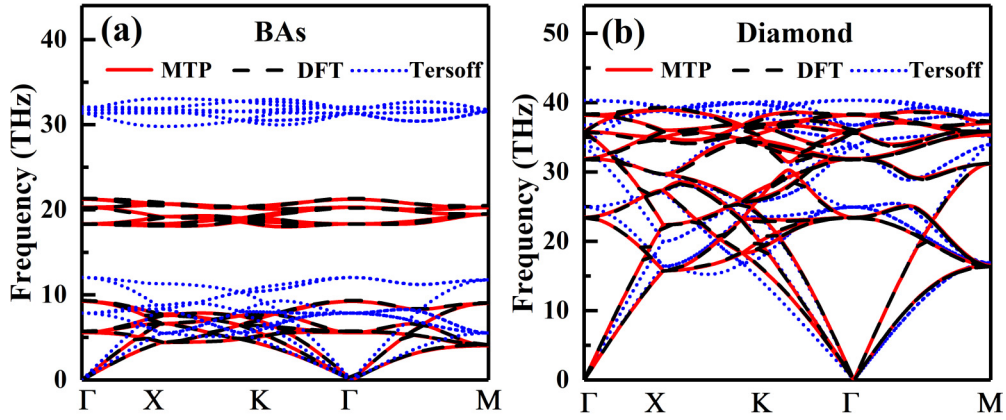
FIG. 2. Phonon dispersion of (a) BAs and (b) diamond along selected high-symmetry path. The solid lines and dashed lines are the results from MTP and DFT calculations, respectively. The dotted lines are the results from Tersoff potential.

distribution of atomic displacement to understand the effect of high-order anharmonicity in BAs and diamond.

To obtain the atomic displacement, EMD simulations are performed on the $8 \times 8 \times 8$ unit cells with periodic boundary conditions, and the time step is set as 0.5 fs. The system is initially equilibrated for 200 ps using the *NVT* ensemble. Then, the system is simulated for another 200 ps under the *NVE* ensemble, and the atomic displacement of each atom in the system is recorded every 5 fs. The probability distribution of atomic displacements for individual atoms can be calculated by dividing the number of occurrences of the atom at a specific displacement by the total recorded steps.

Our simulation results show that the probability distribution of atomic displacement is isotropic among different directions (see Fig. S2 in Supplemental Material [48]). Therefore, following the style used in Ref. [52], we plot in Fig. 3(a) the probability distribution of atomic displacement along the x direction in BAs and diamond at different temperatures. Obviously, the center of the probability distribution remains at the equilibrium position for both BAs and diamond. We can see that the maximum amplitude of atomic displacement in BAs [stars in Fig. 3(a)] is notably larger than that in diamond [squares in Fig. 3(a)]. This indicates that BAs has a stronger anharmonicity than diamond under the same temperature condition. Moreover, the atomic displacement of both BAs and diamond increases with increasing temperature.

When the atomic amplitude exceeds the harmonic approximation, its potential-energy surface can no longer be described only by the second-order Taylor expansion. As a result, the corrections by the higher-order terms should be considered, which induces the anharmonic force acting on the atoms. In general, as temperature rises, stronger Umklapp phonon scattering and higher-order anharmonic phonon scattering are introduced, resulting in the decrease of thermal conductivity. Therefore, considering anharmonic phonon characteristics at high temperatures is critical to ensure the accuracy of thermal conductivity prediction.

From Fig. 3(a), we can see that at a given temperature, the probability distribution reveals that most displacement is small, while the large displacement exists with a lower probability. In order to assess the importance of anharmonic force, we calculate for each temperature both the harmonic

force based on the harmonic force constant and the real force which contains the anharmonic interactions and can be obtained directly from MD simulations. At each temperature, the maximum displacement ($u_{\max}$) from the probability distribution is used as the input data for the force calculations. More specifically, we set the displacement of atom i in the system to $u_{\max}^{\alpha}$ (α is the Cartesian coordinate index). At the same time, the rest of the atoms are still in their equilibrium positions. Based on the harmonic approximation, the harmonic force for atom i along the α direction $F_{i\_\text{har}}^{\alpha}$ is computed as

$$F_{i\_\text{har}}^{\alpha} = \left| \sum_{j \neq i}^{N} \sum_{\beta = x,y,z} k_{ij}^{\alpha\beta} \times u_{\max}^{\alpha} \right|, \qquad (10)$$

where N represents the total number of atoms in the systems, and $k_{ij}^{\alpha\beta}$ is the 2-rd IFCs. The ensemble-averaged harmonic force in the system is defined as

$$F_{\text{ave\_har}} = \frac{1}{3N} \sum_{\alpha = x,y,z} \sum_{i=1}^{N} F_{i\_\text{har}}^{\alpha}. \qquad (11)$$

On the other hand, based on MD simulations with MTP, we calculate the real force $F_{i\_\text{real}}^{\alpha}$ of atom i. Similarly, the ensemble-averaged real force in the system $F_{\text{ave\_real}}$ can be obtained by averaging over different atoms and Cartesian coordinates. Finally, we quantify the relative contribution of anharmonic force by calculating the ratio W_{anhar}:

$$W_{\text{anhar}} = \left| \frac{F_{\text{ave\_real}} - F_{\text{ave\_har}}}{F_{\text{ave\_real}}} \right|. \qquad (12)$$

The averaged harmonic force $F_{\text{ave\_har}}$ and real force $F_{\text{ave\_real}}$, as well as the ratio of anharmonic force W_{anhar} for BAs and diamond are shown in Figs. 3(b) and 3(c), respectively. We find that $F_{\text{ave\_har}}$ increases almost linearly with the increase of temperature. Moreover, $F_{\text{ave\_real}}$ overlaps with $F_{\text{ave\_har}}$ at low temperature (below 100 K), but the difference between them becomes more significant with increasing temperature, suggesting the deviation from the harmonic approximation at elevated temperature. Furthermore, by comparing W_{anhar} values in BAs and diamond, we can find that the relative contribution of anharmonic force in BAs is obviously larger than that in diamond, which indicates that BAs have a stronger
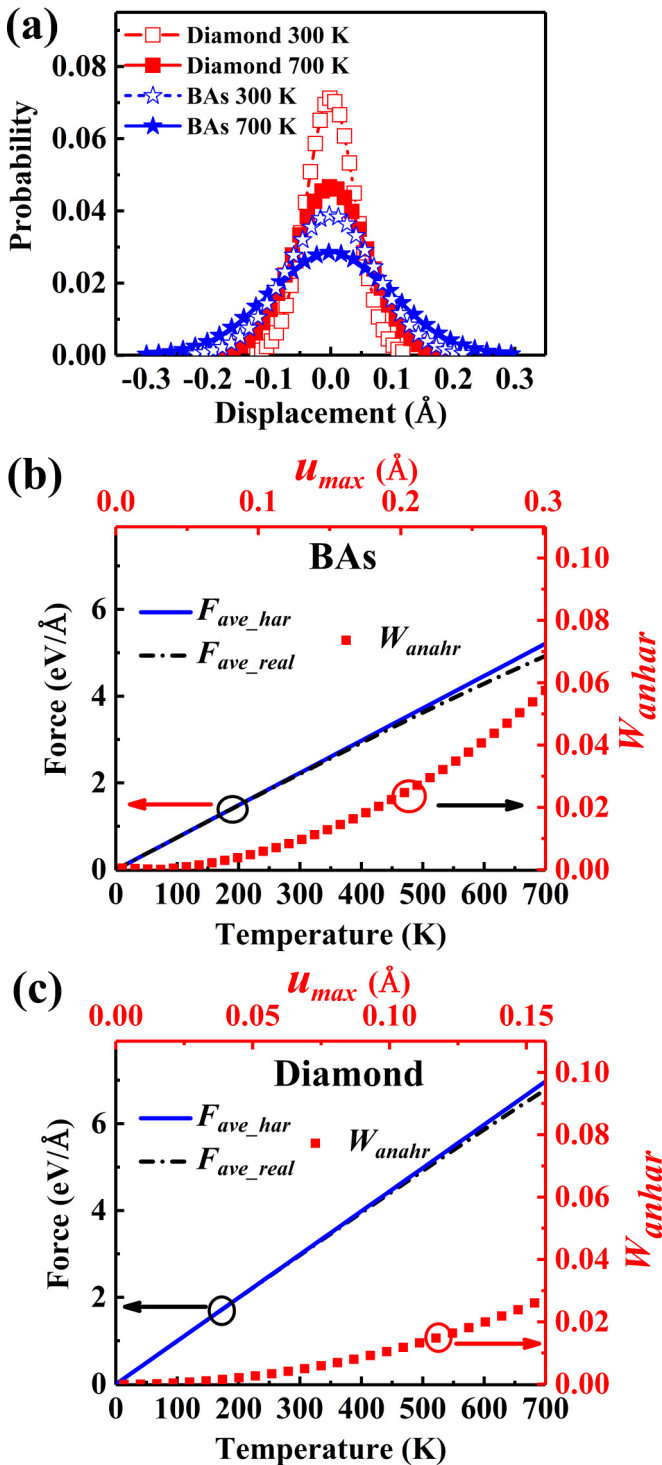
FIG. 3. (a) Probability distributions of atomic displacements along the x direction calculated from MD simulations combined with MTP for BAs and diamond at 300 and 700 K. (b) and (c) show the average harmonic force (F_{ave_har}), average real force (F_{ave_real}), and the weight of anharmonic force (W_{anhar}) for BAs and diamond, respectively.

lattice anharmonicity than diamond, especially at high temperature.

The relationship between W_{anhar} and temperature suggests that the anharmonic atomic force increases as temperature

rises. Our results also show that at low temperature, it is reasonable to use the harmonic force as the approximation of the real force of atoms (i.e., harmonic approximation). However, as the temperature increases, the atomic displacement deviates substantially away from the equilibrium position, which introduces significant anharmonic forces and thus causes the failure of the harmonic approximation.

2. Spectral energy density analysis

Compared to the phonon dispersion computed by lattice dynamics calculations, SED contains additional information about the linewidth of individual phonons at finite temperatures, which reflects the lattice anharmonicity in crystals. To this end, we show in Fig. 4 the SED contour plot for BAs and diamond at finite temperatures. The colormap in Fig. 4 denotes the vibrational energy spectrum distribution for various phonon wave vectors and frequencies, and the green solid line represents the harmonic phonon dispersion at 0 K obtained from DFT calculations. The overall shape of phonon dispersion calculated by SED agrees quite well with results from the DFT calculations, which again highlights the accuracy of MTP used in MD simulation. Moreover, a pronounced mode softening for the optical phonons is observed in both materials at finite temperatures compared to the DFT results at 0 K. Besides, the acoustic phonons modes also undergo a relatively small shift to the lower frequencies with increasing temperature, especially for BAs at high temperatures [Fig. 4(c)]. This temperature-induced mode softening is consistent with previous temperature-dependent effective potential method calculations [53,54] and phonon renormalization theory [55].

In addition to the temperature effect on the phonon frequency, the strength of anharmonic phonon-phonon interaction is also enhanced with increasing temperature, which leads to the broadening of phonon mode at finite temperatures. This point can be seen in Fig. 4 that the phonon linewidths in both BAs and diamond become wider as temperature rises from 300 to 700 K. Moreover, Fig. 4 further reveals that the phonon linewidth in BAs (left panels) is notably wider than that in diamond (right panels) at the same temperature, especially for the optical phonons. Therefore, SED analysis further confirms that the lattice anharmonicity in BAs is stronger than that in diamond at the same temperature, which is consistent with the atomic displacement results shown in Fig. 3.

D. Thermal conductivity

We have examined the validity of using MTP for describing the effects of lattice anharmonicity and temperature in MD simulation. To further examine its validity in predicting the macroscopic thermal transport property, we finally compute κ of both BAs and diamond based on MTP. In this regard, we first use the same method, PBTE framework considering only 3ph scattering process, to calculate κ based on 2-rd and 3-rd IFCs computed from MTP and DFT calculations. Furthermore, the PBTE predictions are also compared with literature results to verify the accuracy of MTP. Moreover, EMD simulations with MTP that include all orders of anharmonicity are also performed to compute κ, and are further compared with PBTE results that only include the 3ph scattering process, in order to highlight the importance of high-order anharmonicity.
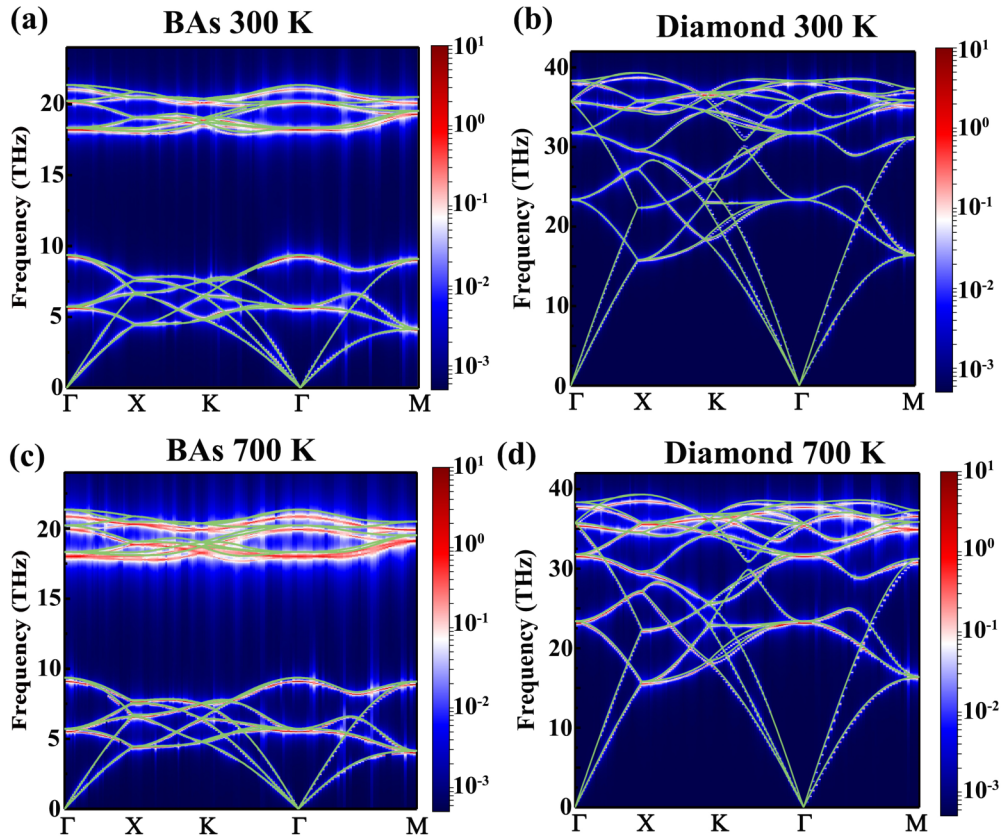
FIG. 4. Spectral energy density calculated by MD simulations combined with MTP along the selected high-symmetry path for BAs at (a) 300 and (c) 700 K, and diamond at (b) 300 and (d) 700 K. The green solid line represents the harmonic phonon dispersion at 0 K from DFT calculations.

1. PBTE framework

Figures 5(a) and 5(b) show our PBTE predictions of κ considering only the 3ph scattering process (solid square and star) as a function of temperature for BAs and diamond, respectively. The previous PBTE calculations by Feng *et al.* [7] considering up to 4ph scattering process (solid circle) and experimental results [16–18] (empty symbols) are also included in Fig. 5 for comparison.

When only considering the 3ph scattering process, our calculation results of room-temperature κ for BAs and diamond based on DFT (solid square in Fig. 5) are 2230 and 2225 $Wm^{-1}K^{-1}$, respectively, and both of them agree well with previous theoretical studies [7,15,56]. Moreover, Fig. 5 further shows that the PBTE predictions of κ based on MTP (solid star) agree quantitatively well with results based on DFT (solid square) in a wide temperature range for both BAs and diamond. In addition, based on PBTE considering 3ph scattering and MTP, we can also evaluate the mode contribution to the total thermal conductivity from different phonon branches, such as transverse acoustic (TA), longitudinal acoustic (LA), and optical branches. For instance, our calculation results reveal that the relative contribution from TA1, TA2, LA, and all optical branches to thermal conductivity of BAs at 300 K is, respectively, 28.12, 47.90, 23.75, and 0.23%, which agrees quantitatively well with previous *ab initio* calculations [13]. These agreements confirm that MTP can provide IFCs with the similar accuracy as DFT for the

prediction of κ, which is consistent with our previous study [32] on graphene with MLP.

The importance of high-order anharmonicity on thermal transport can be revealed by comparing thermal conductivity results with and without the 4ph scattering process. Figure 5(a) further shows that for BAs, our PBTE prediction of κ is significantly higher than the predictions by Feng *et al.* [7] that include the 4ph scattering process (solid circle) and the experimental results (empty symbols). On the other hand, such difference is negligible for diamond, as shown in Fig. 5(b). This is because the band gap between acoustic and optical phonons in BAs is substantially larger than that in diamond (Fig. 4). Due to this large band gap, some of the phonon scattering channels, which are forbidden by the 3ph process due to the constraint of energy conservation, are allowed in the 4ph process with the participation of an additional phonon. Consequently, the 4ph scattering rate in BAs is significantly enhanced at high temperatures [7], leading to the notably reduced κ in BAs when further considering the 4ph scattering process.

However, the inclusion of high-order anharmonicity in PBTE framework is extremely challenging due to the huge computational load. For example, when using the finite displacement method to calculate the IFCs matrix, atomic forces from different supercell configurations are needed to compute each element in the IFCs matrix. The total number of element in third-order IFCs and four-order IFCs are $27n^3\mathbb{N}^2$ and
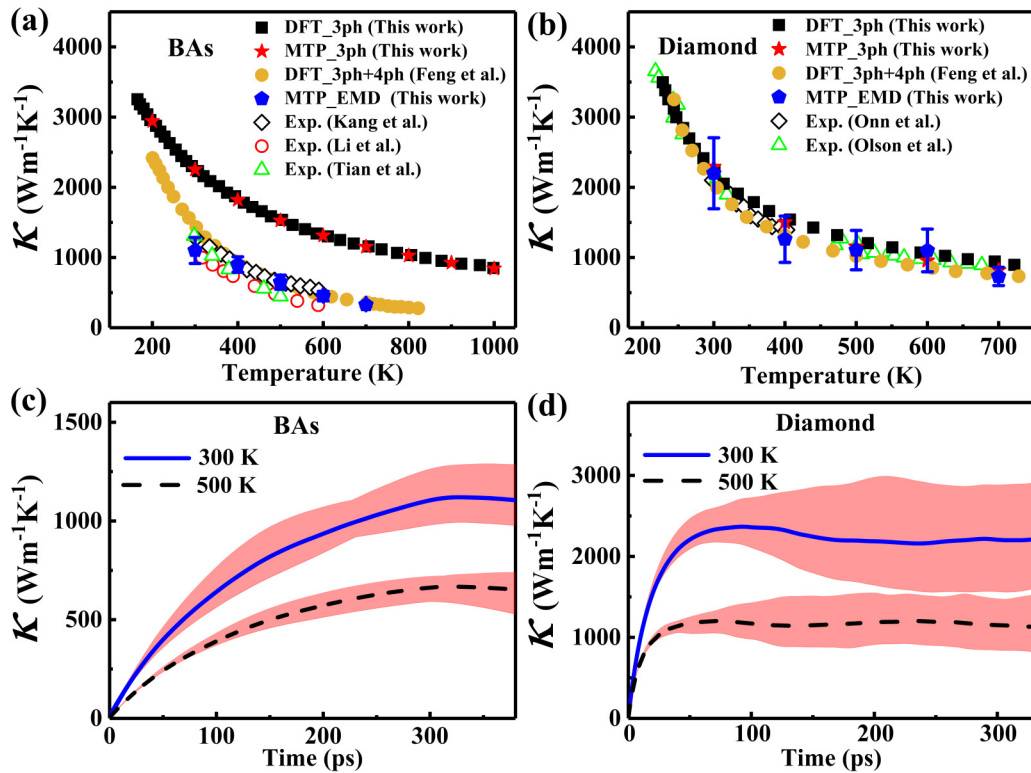
FIG. 5. Lattice thermal conductivity κ of BAs and diamond. (a) and (b) show, respectively, κ of BAs and diamond vs temperature from theoretical predictions (solid symbols) and experimental measurements (empty symbols). The solid square and star denote predictions in this work by PBTE framework considering only 3ph process with force constants from DFT and MTP, respectively, while the solid pentagon draws the predictions in this work by EMD with MTP. The solid circle denotes literature results by Feng *et al.* [7] considering both 3ph and 4ph processes for BAs and diamond. The empty symbols draw the experimental results in literature studies from Kang *et al.* [16], Li *et al.* [17], and Tian *et al.* [18] for BAs, and from Onn *et al.* [58] and Olson *et al.* [59] for diamond. (c) and (d) show the predicted thermal conductivity by Green-Kubo method with MTP vs integration time for BAs and diamond, respectively. The solid and dashed lines represent the averaged thermal conductivity over 30 independent simulations, and the shadowed area represents the corresponding deviation.

$81n^4\mathbb{N}^3$, respectively. Here, n denotes the number of atoms in a unit cell and $\mathbb{N}$ denotes the number of unit cells. Therefore, it is computationally expensive to obtain the atomic forces based on DFT calculations for the calculation of the high-order IFCs. Furthermore, when studying a new material, it is in practice not possible to determine *a priori* whether high-order anharmonic phonon interactions (e.g., 4ph, or even higher) should be considered in prediction of κ, unless complicated and expensive calculations are carried out. Since it is computationally challenging to consider the higher-order phonon scattering processes based on PBTE framework, a different framework beyond the perturbative approach in PBTE to consider the high-order anharmonicity or even full order anharmonicity is highly desirable for the accurate prediction of lattice thermal conductivity.

2. Green-Kubo formulism

MD simulations, on the other hand, can implicitly include anharmonicity to all orders via the realistic interatomic potential. To this end, we finally use the Green-Kubo method combined with MTP to assess the intrinsic κ of BAs and diamond.

Figures 5(c) and 5(d) show, respectively, the prediction of κ for BAs and diamond by the Green-Kubo formula versus

integration time at two representative temperatures. The solid and dashed lines draw the averaged κ over 30 independent simulations at 300 and 500 K, respectively, while the shadowed region indicates the uncertainty range of κ. More EMD simulation results at different temperatures are shown in Fig. S3 in the Supplemental Material [48]. A convergent trend for the averaged κ is observed for both BAs and diamond when the integration time is sufficiently long. For BAs, we obtain $\kappa = 1100 \pm 125 \, \mathrm{Wm^{-1}K^{-1}}$ and $\kappa = 648 \pm 61 \, \mathrm{Wm^{-1}K^{-1}}$ at 300 and 500 K, respectively. Although Figs. 5(c) and 5(d) show the uncertainty of κ decreases at higher temperature (presumably due to the reduced κ value with increasing temperature), we find the relative uncertainty (uncertainty of κ devided by κ) exhibits no obvious dependence on temperature for both BAs and diamond, suggesting that temperature has almost no impact on the relative error in EMD simulations. This result is consistent with the theoretical study by Wang *et al.* [57] on the uncertainty analysis of EMD simulations.

As shown in Fig. 5(a), the predicted κ of BAs by EMD simulations combined with MTP agrees reasonably well with the experimental values [16–18] and *ab initio* calculations [7] containing the 4ph scattering process recorded in literature in a wide temperature range. Based on the same MTP, our EMD predictions of κ are obviously lower than our PBTE predictions that only consider the 3ph scattering process, which

further confirms that high-order anharmonicity is quite important for thermal transport in BAs and can be well captured by MD simulation. For diamond, a good agreement between the EMD predictions with MTP and experimental results [58,59] at various temperatures is observed in Fig. 5(b). Besides, the difference between EMD and 3ph limited PBTE predictions is very small in diamond, suggesting that the impact of high-order anharmonicity is relatively weak in diamond compared to BAs. Therefore, these comparisons in Fig. 5 demonstrate that EMD simulation combined with MTP is capable of accurate prediction of a material's κ, regardless of whether high-order lattice anharmonicity is important or not in various crystals.

Although the κ values of BAs and diamond have been reported in previous studies, performing systematic calculations on these materials based on different theoretical frameworks allows us to highlight the advantages of MD simulations combined with MLP for describing the effects of high-order anharmonicity and temperature on thermal transport in different materials. As demonstrated above, the accuracy of MD simulations with MTP used in this study appears to be comparable to experimental measurements and/or DFT calculations. Moreover, the MD method includes full order anharmonicity and thus requires no *a priori* knowledge on whether high-order phonon scattering process is important, which is a quite challenging task in the perturbative treatment of anharmonicty in PBTE framework. More importantly, MD simulations allow for the modeling of realistic factors, such as disorder, defect, and finite temperature effect, which are otherwise difficult to be handled in DFT calculations. Therefore, from a methodological perspective, we believe that MD simulation combined with MLP is a powerful technique for studying the temperature effect and high-order anharmonicity on thermal transport in realistic materials.

IV. CONCLUSION

In summary, we have explored the capabilities of MD simulations combined with MLP in studying the high-order phonon anharmonicity and thermal conductivity of BAs and diamond. The trained MTP can predict the energy, atomic force, and phonon dispersion with a high accuracy comparable to that of DFT calculations for both BAs and diamond. In contrast, the consistency between the DFT calculations and commonly used Tersoff potential is relatively poor for the phonon dispersion. Moreover, both the amplitude of atomic displacement and phonon broadening effect reveal a stronger lattice anharmonicity in BAs than that in diamond at the same temperature. For the thermal conductivity, Green-Kubo framework combined with MTP predicts the κ at different temperatures in good agreement with experimental results for both BAs and diamond. In contrast, the PBTE framework only considering the 3ph process substantially overestimates the κ of BAs, regardless of using IFC based on DFT or MTP, due to the non-negligible role of high-order phonon scattering process in BAs. Our study suggests that MD simulations combined with MLP open an avenue beyond the perturbative approach in the PBTE framework to accurately account for the full orders of anharmonicity, and have been demonstrated as a powerful tool to evaluate the lattice thermal conductivity of various crystals without the *a priori* knowledge of the importance of high-order phonon anharmonicity.

[1] Z. Zhang, Y. Ouyang, Y. Cheng, J. Chen, N. Li, and G. Zhang, Phys. Rep. **860**, 1 (2020).

[2] Z. Zhang, Y. Guo, M. Bescond, J. Chen, M. Nomura, and S. Volz, Phys. Rev. B **103**, 184307 (2021).

[3] W. Ren, Y. Ouyang, P. Jiang, C. Yu, J. He, and J. Chen, Nano Lett. **21**, 2634 (2021).

[4] Y. Fu, J. Hansson, Y. Liu, S. Chen, A. Zehri, M. K. Samani, N. Wang, Y. Ni, Y. Zhang, Z.-B. Zhang, Q. Wang, M. Li, H. Lu, M. Sledzinska, C. M. S. Torres, S. Volz, A. A. Balandin, X. Xu, and J. Liu, 2D Mater. **7**, 012001 (2019).

[5] Y.-J. Zeng, D. Wu, X.-H. Cao, W.-X. Zhou, L.-M. Tang, and K.-Q. Chen, Adv. Funct. Mater. **30**, 1903873 (2020).

[6] Y. Ouyang, Z. Zhang, D. Li, J. Chen, and G. Zhang, Ann. Phys. **531**, 1800437 (2019).

[7] T. Feng, L. Lindsay, and X. Ruan, Phys. Rev. B **96**, 161201 (2017).

[8] X. Gu, Z. Fan, H. Bao, and C. Y. Zhao, Phys. Rev. B **100**, 064306 (2019).

[9] T. Feng and X. Ruan, Phys. Rev. B **97**, 045202 (2018).

[10] Z. Zhang, S. Hu, J. Chen, and B. Li, Nanotechnology **28**, 225704 (2017).

[11] S. Chen, Q. Wu, C. Mishra, J. Kang, H. Zhang, K. Cho, W. Cai, A. A. Balandin, and R. S. Ruoff, Nat. Mater. **11**, 203 (2012).

[12] S. Hu, J. Chen, N. Yang, and B. Li, Carbon **116**, 139 (2017).

[13] X. Yang, T. Feng, J. Li, and X. Ruan, Phys. Rev. B **100**, 245203 (2019).

[14] A. Kundu, X. Yang, J. Ma, T. Feng, J. Carrete, X. Ruan, G. K. H. Madsen, and W. Li, Phys. Rev. Lett. **126**, 115901 (2021).

[15] L. Lindsay, D. A. Broido, and T. L. Reinecke, Phys. Rev. Lett. **111**, 025901 (2013).

[16] J. S. Kang, M. Li, H. Wu, H. Nguyen, and Y. Hu, Science **361**, 575 (2018).

[17] S. Li, Q. Zheng, Y. Lv, X. Liu, X. Wang, P. Y. Huang, D. G. Cahill, and B. Lv, Science **361**, 579 (2018).

[18] F. Tian, B. Song, X. Chen, N. K. Ravichandran, Y. Lv, K. Chen, S. Sullivan, J. Kim, Y. Zhou, T.-H. Liu, M. Goni, Z. Ding, J. Sun, G. A. G. U. Gamage, H. Sun, H. Ziyaee, S. Huyan, L. Deng, J. Zhou, A. J. Schmidt, S. Chen, C.-W. Chu, P. Y. Huang, D. Broido, L. Shi, G. Chen, and Z. Ren, Science **361**, 582 (2018).

[19] B. Mortazavi, E. V. Podryabinkin, I. S. Novikov, T. Rabczuk, X. Zhuang, and A. V. Shapeev, Comput. Phys. Commun. **258**, 107583 (2021).

[20] Z. Liu, X. Yang, B. Zhang, and W. Li, ACS Appl. Mater. Interfaces **13**, 53409 (2021).

[21] Z. Zhang, J. Chen, and B. Li, Nanoscale **9**, 14208 (2017).

[22] Z. Zhang, S. Hu, T. Nakayama, J. Chen, and B. Li, Carbon **139**, 289 (2018).

[23] S. Hu, Z. Zhang, P. Jiang, W. Ren, C. Yu, J. Shiomi, and J. Chen, Nanoscale **11**, 11839 (2019).

[24] P. Jiang, Y. Ouyang, W. Ren, C. Yu, J. He, and J. Chen, APL Mater. **9**, 040703 (2021).

[25] P. K. Schelling, S. R. Phillpot, and P. Keblinski, Phys. Rev. B **65**, 144306 (2002).

[26] J. E. Turney, A. J. H. McGaughey, and C. H. Amon, Phys. Rev. B **79**, 224305 (2009).

[27] Y. Ouyang, C. Yu, G. Yan, and J. Chen, Front. Phys. **16**, 43200 (2021).

[28] I. I. Novoselov, A. V. Yanilkin, A. V. Shapeev, and E. V. Podryabinkin, Comput. Mater. Sci. **164**, 46 (2019).

[29] P. Rowe, G. Csányi, D. Alfè, and A. Michaelides, Phys. Rev. B **97**, 054303 (2018).

[30] V. L. Deringer, M. A. Caro, and G. Csányi, Adv. Mater. **31**, 1902765 (2019).

[31] H. Liu, X. Qian, H. Bao, C. Y. Zhao, and X. Gu, J. Phys.: Condens. Matter **33**, 405401 (2021).

[32] Y. Ouyang, Z. Zhang, C. Yu, J. He, G. Yan, and J. Chen, Chin. Phys. Lett. **37**, 126301 (2020).

[33] G. Kresse and J. Furthmüller, Comput. Mater. Sci. **6**, 15 (1996).

[34] G. Kresse and D. Joubert, Phys. Rev. B **59**, 1758 (1999).

[35] A. V. Shapeev, Multiscale Model. Simul. **14**, 1153 (2016).

[36] Y. Zuo, C. Chen, X. Li, Z. Deng, Y. Chen, J. Behler, G. Csanyi, A. V. Shapeev, A. P. Thompson, M. A. Wood, and S. P. Ong, J. Phys. Chem. A **124**, 731 (2020).

[37] I. S. Novikov, K. Gubaev, E. V. Podryabinkin, and A. V. Shapeev, Mach. Learn.: Sci. Technol. **2**, 025002 (2021).

[38] A. Togo and I. Tanaka, Scr. Mater. **108**, 1 (2015).

[39] W. Li, J. Carrete, N. A. Katcho, and N. Mingo, Comput. Phys. Commun. **185**, 1747 (2014).

[40] J. He, Y. Ouyang, C. Yu, P. Jiang, W. Ren, and J. Chen, Chin. Phys. B **29**, 126503 (2020).

[41] W. Ren, Z. Zhang, C. Chen, Y. Ouyang, N. Li, and J. Chen, Front. Mater. **7**, 569090 (2020).

[42] S. Plimpton, J. Comput. Phys. **117**, 1 (1995).

[43] R. Kubo, J. Phys. Soc. Jpn. **12**, 570 (1957).

[44] J. Chen, G. Zhang, and B. Li, Phys. Lett. A **374**, 2392 (2010).

[45] M. S. Green, J. Chem. Phys. **22**, 398 (1954).

[46] Z. Fan, L. F. C. Pereira, H.-Q. Wang, J.-C. Zheng, D. Donadio, and A. Harju, Phys. Rev. B **92**, 094301 (2015).

[47] J. Larkin, J. Turney, A. Massicotte, C. Amon, and A. McGaughey, J. Comput. Theor. Nanosci. **11**, 249 (2014).

[48] See Supplemental Material at http://link.aps.org/supplemental/10.1103/PhysRevB.105.115202 for the accuracy of MTP trained with larger training data in predicting energy and atomic force of BAs and diamond, the three-dimensional plot for the probability distribution of atomic displacement of BAs and diamond at different temperatures, and the predicted thermal conductivity of BAs and diamond at different temperatures by EMD simulations.

[49] J. Tersoff, Phys. Rev. B **37**, 6991 (1988).

[50] F. Benkabou, C. Chikr.Z, H. Aourag, P. J. Becker, and M. Certier, Phys. Lett. A **252**, 71 (1999).

[51] L. Shi, X. Ma, M. Li, Y. Zhong, L. Yang, W. Yin, and X. He, Phys. Chem. Chem. Phys. **23**, 8336 (2021).

[52] Y. Lu, T. Sun, and D. B. Zhang, Phys. Rev. B **97**, 174304 (2018).

[53] O. Delaire, K. Marty, M. B. Stone, P. R. C. Kent, M. S. Lucas, D. L. Abernathy, D. Mandrus, and B. C. Sales, Proc. Natl. Acad. Sci. **108**, 4725 (2011).

[54] J. M. Skelton, S. C. Parker, A. Togo, I. Tanaka, and A. Walsh, Phys. Rev. B **89**, 205203 (2014).

[55] J. S. Kang, H. Wu, M. Li, and Y. Hu, Nano Lett. **19**, 4941 (2019).

[56] D. A. Broido, L. Lindsay, and T. L. Reinecke, Phys. Rev. B **88**, 214303 (2013).

[57] Z. Wang, S. Safarkhani, G. Lin, and X. Ruan, Int. J. Heat Mass Transfer **112**, 267 (2017).

[58] D. G. Onn, A. Witek, Y. Z. Qiu, T. R. Anthony, and W. F. Banholzer, Phys. Rev. Lett. **68**, 2806 (1992).

[59] J. R. Olson, R. O. Pohl, J. W. Vandersande, A. Zoltan, T. R. Anthony, and W. F. Banholzer, Phys. Rev. B **47**, 14850 (1993).